



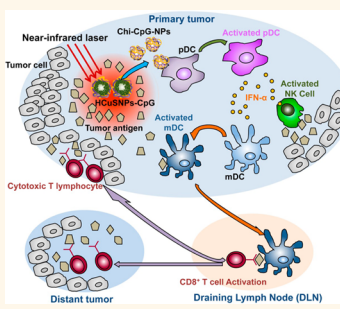
# Combinatorial Photothermal and Immuno Cancer Therapy Using Chitosan-Coated Hollow Copper Sulfide Nanoparticles

Liangran Guo,<sup>†</sup> Daisy D. Yan,<sup>†</sup> Dongfang Yang,<sup>†</sup> Yajuan Li,<sup>†</sup> Xiaodong Wang,<sup>†</sup> Olivia Zalewski,<sup>†</sup> Bingfang Yan,<sup>†</sup> and Wei Lu<sup>†,‡,\*</sup>

<sup>†</sup>Department of Biomedical and Pharmaceutical Sciences, College of Pharmacy, The University of Rhode Island, Kingston, Rhode Island 02881, United States

<sup>‡</sup>School of Pharmacy, Fudan University, Shanghai 201203, China

**ABSTRACT** Near-infrared light-responsive inorganic nanoparticles have been shown to enhance the efficacy of cancer photothermal ablation therapy. However, current nanoparticle-mediated photothermal ablation is more effective in treating local cancer at the primary site than metastatic cancer. Here, we report the design of a near-infrared light-induced transformative nanoparticle platform that combines photothermal ablation with immunotherapy. The design is based on chitosan-coated hollow CuS nanoparticles that assemble the immunoadjuvants oligodeoxynucleotides containing the cytosine-guanine (CpG) motifs. Interestingly, these structures break down after laser excitation, reassemble, and transform into polymer complexes that improve tumor retention of the immunotherapy. In this “photothermal immunotherapy” approach, photothermal ablation-induced tumor cell death reduces tumor growth and releases tumor antigens into the surrounding milieu, while the immunoadjuvants potentiate host antitumor immunity. Our results indicated that combined photothermal immunotherapy is more effective than either immunotherapy or photothermal therapy alone against primary treated and distant untreated tumors in a mouse breast cancer model. These hollow CuS nanoparticles are biodegradable and can be eliminated from the body after laser excitation.



**KEYWORDS:** hollow CuS nanoparticle · photothermal · immunotherapy · cancer · cytosine-guanine

Photothermal ablation therapy, employing photoabsorbers and near-infrared light energy sources, provides a precise and minimally invasive alternative for cancer treatment.<sup>1,2</sup> In the past decade, near-infrared light-responsive inorganic nanoparticles, such as gold nanoparticles,<sup>3–7</sup> carbon nanotubes,<sup>8</sup> and CuS nanoparticles,<sup>9–13</sup> have been shown to efficiently convert optical energy into thermal energy and enhance the efficacy of photothermal ablation therapy. Some applications are under clinical trials.<sup>14,15</sup> However, nanoparticle-mediated photothermal ablation, in currently used forms, is employed primarily as a local cancer treatment at the primary site. It is less effective in controlling metastatic cancer.

An ideal cancer photothermal therapy should not only eradicate the treated primary tumors but also induce a systemic

antitumor immunity, capable of controlling metastatic tumors and long-term tumor resistance.<sup>16</sup> One promising strategy is to combine photothermal therapy with immunotherapy.<sup>16,17</sup> It is well-known that tumor cells usually do not induce potent antitumor immune responses because of their inefficient expression of molecules important for antigen processing and presentation.<sup>18</sup> Laser-induced tumor cell death, on the other hand, can release tumor antigens into the surrounding milieu. Concomitantly, immunoadjuvants for cancer immunotherapy promote antigen uptake and presentation by professional antigen-presenting cells, thus triggering specific antitumor immunity.<sup>16</sup> Therefore, photothermal therapy may act synergistically with immunotherapy to enhance immune responses, rendering the tumor residues and metastases more susceptible to immune-mediated killing.

\* Address correspondence to weilu@uri.edu.

Received for review January 13, 2014 and accepted May 6, 2014.

Published online May 06, 2014  
10.1021/nn5002112

© 2014 American Chemical Society

Among immunoadjuvants, oligodeoxynucleotides containing cytosine-guanine (CpG) motifs are efficient modulators of cancer immunotherapy.<sup>19</sup> They specifically activate Toll-like receptor 9 signaling in plasmacytoid dendritic cells, a type of key regulatory cell for the activation of innate and adaptive immune responses.<sup>19–21</sup> CpG oligodeoxynucleotides can be effective as monotherapy and as vaccine adjuvants for cancer treatment.<sup>22–24</sup> However, clinical use of CpG oligodeoxynucleotides faces several challenges including *in vivo* instability, unfavorable pharmacokinetic and biodistribution characteristics, and a requirement for intracellular uptake because Toll-like receptor 9 is located in the endosomal compartment.<sup>25</sup> Recent studies indicate that nanoparticles can promote CpG uptake into Toll-like receptor 9-rich endosomes of plasmacytoid dendritic cells, thus improving efficacy.<sup>26–35</sup>

In this study, we report the design of CuS-based, light-induced transformative nano-CpG systems that combine photothermal ablation with immunotherapy. We have recently reported that hollow CuS nanoparticles (HCuSNPs) are biodegradable photothermal coupling agents that can be excreted from liver and kidney and have low toxicity.<sup>36</sup> Unlike gold nanorods or hollow gold nanospheres that fuse into solid gold nanoparticles upon near-infrared laser irradiation,<sup>37–40</sup> we have observed, here, that the polycrystalline HCuSNPs undergo disintegration from CuS shells into single CuS crystals after laser treatment. On the basis of this unique characteristic, we have developed chitosan-coated HCuSNPs that assemble the CpG oligodeoxynucleotides for “photothermal immunotherapy” in a mouse breast cancer model. After laser excitation, these structures break down, reassemble, and transform into polymer complexes that enhance CpG tumor retention and uptake by plasmacytoid dendritic cells. The HCuSNPs-mediated photothermal immunotherapy, compared with immunotherapy or photothermal therapy alone, exhibits more potent innate and adaptive immune responses, resulting in combined anticancer effects against primary treated and distant untreated tumors. These HCuSNPs are biodegradable and can be eliminated from the body after laser irradiation.

## RESULTS AND DISCUSSION

Transmission electron microscopic imaging showed that HCuSNPs were on average 85 nm in diameter with hollow interiors (Figure 1A). The nanoparticle shell was porous and composed of small crystals of 10–12 nm in diameter (Figure 1A, arrows). According to the Kirkendall effect, these CuS crystals formed on the outside and inside surfaces of the nanoparticle's shell through sulfidation.<sup>41</sup> The holes in the shell became a shortcut for mass diffusion and transference. Interestingly, following irradiation with a pulsed near-infrared laser ( $2.0 \text{ W/cm}^2$ , 40 s) at 900 nm, the HCuSNPs broke down

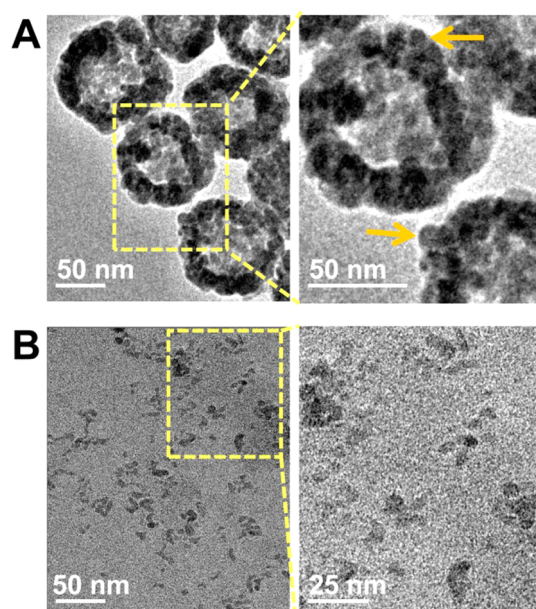


**Figure 1.** Transmission electron microscopic imaging of (A) HCuSNPs composed of small CuS nanocrystals (arrows) and (B) small CuS nanoparticles as a result of disintegration of HCuSNPs following near-infrared laser ( $2.0 \text{ W/cm}^2$ , 40 s, 900 nm) irradiation.

into small CuS nanoparticles between 7 and 12 nm in diameter (Figure 1B), indicating photothermally induced disintegration from original polycrystalline CuS shells into single CuS crystals.

The schematic diagram in Figure 2A illustrates the near-infrared light-induced transformative nano-CpG systems based on HCuSNPs as photothermal coupling elements. The systems assemble through chitosan surface coating on HCuSNPs *via* a disulfide bond followed by CpG condensation to form HCuSNPs-chitosan-CpG (HCuSNPs-CpG) conjugates. Specifically, the laser-triggered disintegration of HCuSNPs separates the disintegrated small CuS nanoparticles from the original HCuSNPs-CpG assembly, subsequently allowing the systems to reassemble and transform into chitosan-CpG nanocomplexes.

Transmission electron microscopic imaging of HCuSNPs-CpG conjugates confirmed that the HCuSNPs' surface was well-coated with chitosan and CpG, forming a 10 nm thick layer (Figure 2B,1). The HCuSNPs-CpG nanoparticles were stable in aqueous solution. However, following near-infrared laser treatment ( $2.0 \text{ W/cm}^2$ , 40 s, 900 nm) and low-speed centrifugation (3000 rpm, 5 min), the CuS nanoparticles precipitated. Transmission electron microscopic examination of the supernatant revealed many nanoparticles with an average size of ~85 nm (Figure 2B,2). These nanoparticles were CuS crystal-deficient in their core, suggesting that HCuSNPs-CpG transformed into chitosan-CpG nanocomplexes. On the other hand, the pellets were identified as disintegrated small CuS nanoparticles without surface coating (Figure 2B,3). This result indicated that

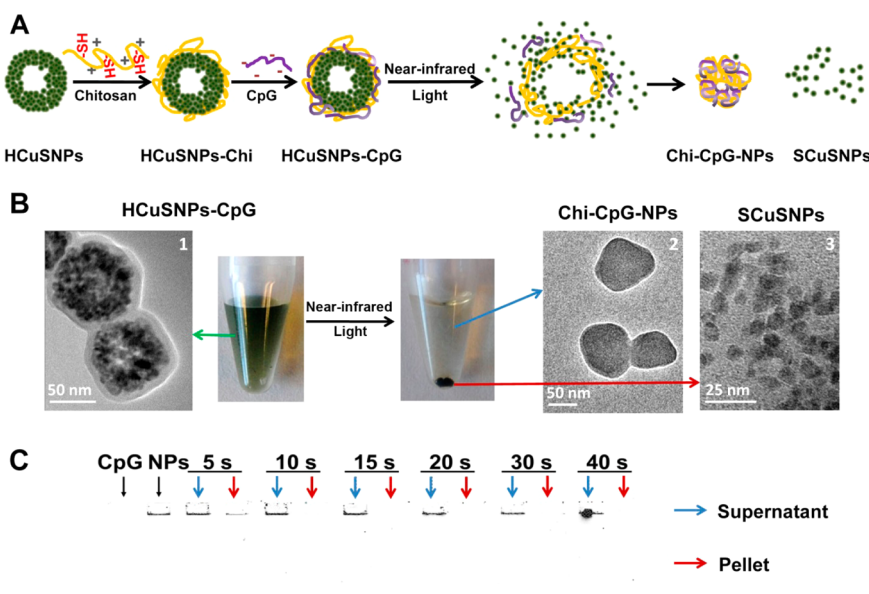


**Figure 2.** (A) Scheme of assembly of HCuSNPs-CpG conjugates, near-infrared light-triggered disintegration of HCuSNPs, and system reassembly. “HCuSNPs-Chi” represents chitosan-coated HCuSNPs. “Chi-CpG-NPs” represents chitosan-CpG nanocomplexes. “SCuSNPs” represents small CuS nanoparticles. (B) Transmission electron microscopic imaging of HCuSNPs-CpG before and after near-infrared laser ( $2.0\text{ W/cm}^2$ , 40 s, 900 nm) treatment and centrifugation (3000 rpm, 5 min). (C) Agarose gel electrophoresis of free CpG, HCuSNPs-CpG before (“NPs”), and after near-infrared laser treatment ( $2.0\text{ W/cm}^2$ ) for different times. Following centrifugation, the supernatant and pellet of each laser-treated sample was individually loaded for electrophoresis.

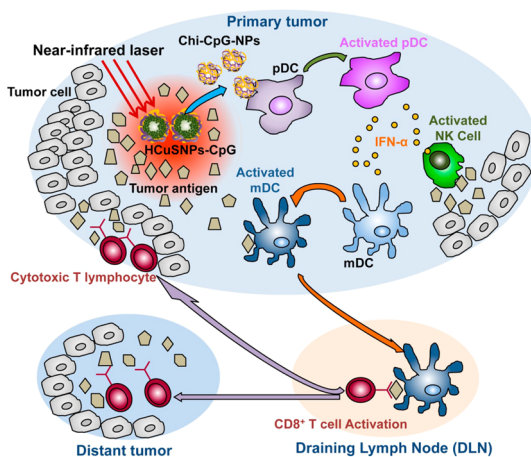
the chitosan polymer detached from the nanoparticles, possibly due to the thermally induced cleavage of disulfide bonds.<sup>42</sup> The disintegrated small CuS nanoparticles precipitated in aqueous solution most likely because of the loss of surface stabilization.

Agarose electrophoresis showed that almost no CpG oligodeoxynucleotides existed in the pellet after laser treatment regardless of the laser exposure time, suggesting that the CpG was completely detached from the HCuSNPs and dispersed in the supernatant (Figure 2C). Analysis of the supernatant revealed that the released CpG existed in both free form and chitosan-CpG nanocomplexes. The latter were formed through CpG condensation by the released chitosan, while the free CpG was ascribed to inadequate amount of chitosan cleaved from the CuS nanoparticles. With increased laser exposure time, the intensity of the free CpG band diminished, reflecting a greater amount of chitosan released to condense CpG. After laser treatment for 40 s, almost all the supernatant CpG was condensed by the released chitosan. There was no detectable band of CpG fragment following the laser treatment.

These results confirmed transformative properties of the near-infrared light-responsive HCuSNPs-CpG conjugates. Accordingly, we hypothesize that intratumorally administrated HCuSNPs-CpG-mediated photothermal ablation, as well as photothermally triggered formation of chitosan-CpG nanocomplexes in primary tumors, effectively elicits systemic immunity against both primary tumors and untreated tumors at a distant

site (Scheme 1). First, the selective photothermal disruption with HCuSNPs can reduce the primary tumor size. Second, the simultaneously photothermal ablation-induced tumor lysis may liberate tumor antigens. Third, chitosan-CpG nanocomplexes, instead of free CpG, may increase stability, tumor retention, and plasmacytoid dendritic cells' internalization of CpG. Through activation of Toll-like receptor 9 signaling, the activated plasmacytoid dendritic cells are able to initiate effective and systemic antitumor immunity through orchestration of an immune cascade.

We first tested if the near-infrared light-triggered formation of chitosan-CpG nanocomplexes resulted in longer tumor retention time than did free CpG. To track CpG oligodeoxynucleotides, we labeled CpG with fluorescent IRDye680 (fCpG) at the 5' terminal *via* an amide linker. BALB/c mice bearing EMT6 murine mammary carcinoma received intratumoral injection of free fCpG or HCuSNPs incorporating fCpG (HCuSNPs-fCpG). Live near-infrared fluorescent imaging showed that the free fCpG was quickly eliminated from tumor 1 h after injection (Figure 3A). After 4 h, there was no fluorescence remaining in the tumor. In contrast, the HCuSNPs-fCpG without laser treatment retained intense fluorescence even 24 h following injection. A similar distribution pattern was evident in mouse intratumorally injected with HCuSNPs-fCpG plus laser irradiation, suggesting that the chitosan-fCpG nanocomplexes had tumor retention capabilities comparable to those of the preformed HCuSNPs-fCpG.



**Scheme 1.** Diagram of HCuSNPs-CpG-mediated photothermal immunotherapy of both primary treated and distant untreated tumors. Under near-infrared laser irradiation, the intratumorally injected HCuSNPs-CpG transform to chitosan-CpG nanocomplexes (Chi-CpG-NPs) resulting in uptake into Toll-like receptor 9-rich endosomes of plasmacytoid dendritic cells (pDCs). Upon stimulation with CpG, the pDCs secrete interferon- $\alpha$  (IFN- $\alpha$ ) to promote innate immunity through NK cell activation. Simultaneously, HCuSNPs-mediated photothermal ablation disrupts the tumor cells, relieving tumor burden and releasing tumor-associated antigens to myeloid dendritic cells (mDCs). In the presence of IFN- $\alpha$  secreted by the activated pDCs, these mDCs become professional antigen-presenting cells and subsequently migrate to tumor-draining lymph nodes (DLNs), where they cross-prime tumor antigen-specific T cells. The antigen-specific CD8 $^{+}$  T cells enter the systemic circulation and are recruited to both primary tumor and untreated tumor at a distant site to trigger the “effector phase” of the adaptive immune response.

Additionally, imaging of dissected tumor-draining lymph nodes (DLN) at 24 h following injection showed that the lymph nodes of the mice treated with HCuSNPs-fCpG plus laser had the strongest fluorescence among the three groups (Figure 3B). This could be attributed to more antigen-presenting cells migrating from tumors to the draining lymph nodes<sup>43</sup> induced by HCuSNPs-fCpG plus laser treatment that carried more fCpG, compared with the other two groups. Fluorescence imaging confirmed significant uptake of fCpG by plasmacytoid dendritic cells 24 h after intratumoral injection of HCuSNPs-fCpG with or without laser treatment (Figure 3C, overlap, yellow). In contrast, there was little fCpG fluorescence 24 h after intratumoral injection of free fCpG. This result demonstrated that the photothermally induced formation of chitosan-CpG nanocomplexes can increase tumor retention of CpG and facilitate its internalization by plasmacytoid dendritic cells.

Previous studies showed that CpG-activated plasmacytoid dendritic cells elicited adaptive immune responses against B16 tumors through activation of NK cells, subsequently leading to maturation of myeloid dendritic cells and cross-priming of tumor antigen-specific cytotoxic T lymphocytes.<sup>43</sup> Here, histological analysis of EMT6 tumors in mice following intratumoral administration of HCuSNPs-CpG plus laser treatment revealed a dramatic infiltration of NK cells (CD49b $^{+}$ ) with expression of the activation marker CD69 compared with saline-treated tumors (Figure 4A, overlap,

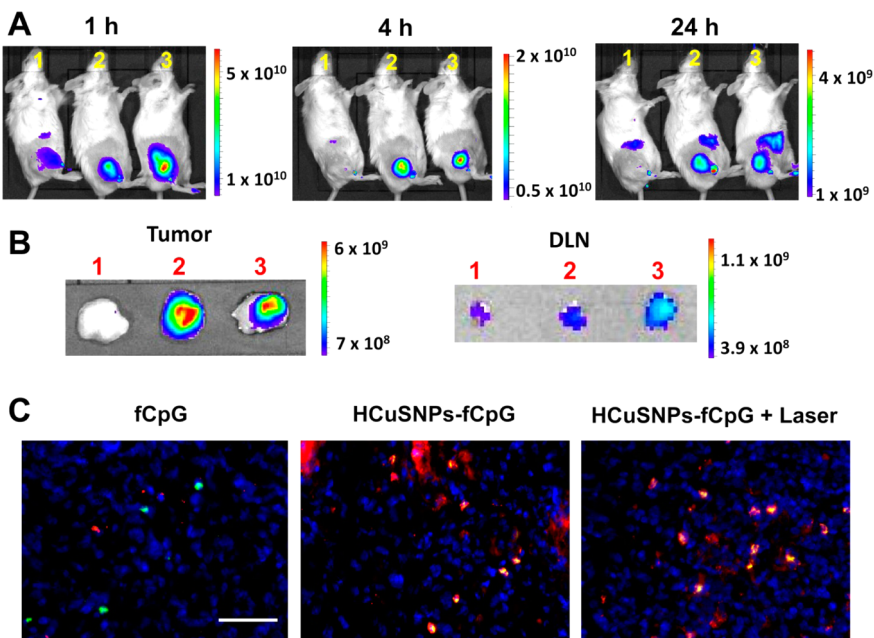


**Figure 3.** (A) Representative live fluorescence imaging of BALB/c mice bearing EMT6 tumors at different time points following intratumoral injection with (1) free fCpG; (2) HCuSNPs-fCpG; or (3) HCuSNPs-fCpG plus laser ( $2.0 \text{ W/cm}^2$ , 40 s, 900 nm). fCpG represents IRDye680-labeled CpG. The injected dose of fCpG in all three groups was  $10 \mu\text{g}/\text{mouse}$ . Fluorescence intensity is expressed as  $\text{p/s/cm}^2/\text{sr}$ . (B) Fluorescence intensity in the dissected tumors and tumor-draining lymph nodes is shown 24 h after administration. (C) Fluorescence micrographs of fCpG distribution in tumors 24 h after intratumoral injection. Pseudored, fCpG; green, mAb (clone 120G8.04)-labeled plasmacytoid dendritic cells; blue, 4',6-diamidino-2-phenylindole (DAPI)-labeled cell nuclei. Scale bar,  $50 \mu\text{m}$ .

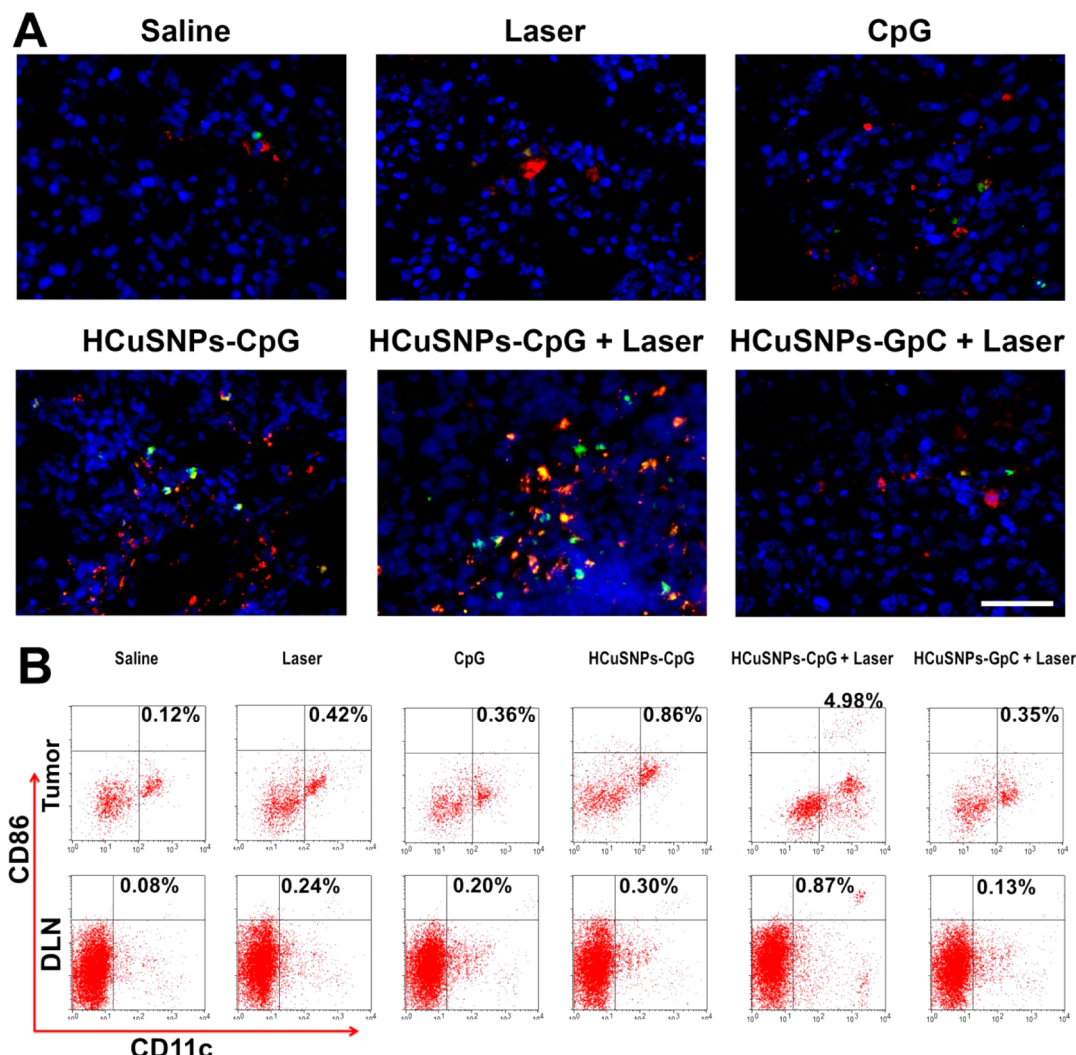


**Figure 4.** EMT6 tumor-bearing mice were given intratumoral injections of saline or different formulations containing  $100\ \mu\text{g}$  of CpG or GpC (sham CpG control) with or without laser treatment ( $2.0\ \text{W}/\text{cm}^2$ ,  $40\ \text{s}$ ,  $900\ \text{nm}$ ) at day 0 and day 6. (A) Tumor sections were stained for activated NK cells ( $\text{CD69}^+\text{CD49b}^+$ ) at day 8. Green, FITC-conjugated anti-mouse CD69; pseudored, allophycocyanin-conjugated anti-mouse CD49b; blue, DAPI. Scale bar,  $50\ \mu\text{m}$ . (B) Flow cytometric analysis of activated myeloid dendritic cells ( $\text{CD11c}^+\text{CD86}^+$ ) in tumors or draining lymph nodes is shown at day 8. “HCuSNPs-GpC” represents HCuSNPs-chitosan-GpC conjugates.

yellow). Intratumoral injection of HCuSNPs-CpG without laser treatment also induced a significant amount of NK cell infiltration but with fewer activated phenotypes than HCuSNPs-CpG plus laser treatment. Tumors treated with free CpG alone or laser alone did not show significant NK cell infiltration. As a control of photothermal therapy alone, we formulated HCuSNPs-chitosan-GpC conjugates (HCuSNPs-GpC) by replacing CpG with GpC oligodeoxynucleotide (sham CpG control). GpC oligodeoxynucleotide contains GpC dinucleotides instead of CpGs and thus does not have Toll-like receptor 9 stimulatory effects.<sup>44</sup> As a result, HCuSNPs-GpC plus laser treatment did not induce NK cell infiltration. Flow cytometric analysis confirmed that HCuSNPs-CpG plus laser treatment induced the highest percentage of the  $\text{CD69}^+$  phenotype in tumors among all treatments (Supporting Information Figure S1). The amount of mature myeloid dendritic cells

( $\text{CD11c}^+\text{CD86}^+$ ) in tumors of mice intratumorally injected with HCuSNPs-CpG plus laser irradiation increased by 41-fold compared with saline-treated control (Figure 4B). This amount was 5.8- and 14.2-fold higher than that in tumors of mice treated with HCuSNPs-CpG alone and HCuSNPs-GpC plus laser, respectively. In addition, the treatment with HCuSNPs-CpG plus laser induced the greatest number of mature myeloid dendritic cells migrating to tumor-draining lymph nodes among all the groups. The population of plasmacytoid dendritic cells in tumors or the draining lymph nodes also increased in mice treated with HCuSNPs-CpG plus laser (Figure S2). Collectively, these results indicated that photothermal ablation and the photothermally triggered formation of chitosan-CpG nanocomplexes have a combined effect on the activation of NK cells and myeloid dendritic cells following intratumoral injection with HCuSNPs-CpG plus laser treatment.

A hallmark of immunotherapy is its success in inducing cytotoxic T lymphocytes, which have the well-documented ability to eradicate tumors *in vivo*.<sup>43</sup> Effector CD8<sup>+</sup> T cells are known to produce IFN- $\gamma$ , which is considered an indicator for T-helper cell 1 (Th1)-type immune responses. We found that HCuSNPs-CpG plus laser treatment induced the largest amount of IFN- $\gamma$ -secreting CD8<sup>+</sup> T cells in tumor-draining lymph nodes among all the treatment groups (Figure 5A). Importantly, the HCuSNPs-CpG plus laser treatment elicited systemic immunity, as evidenced by the significantly increased amount of IFN- $\gamma$ -secreting CD8<sup>+</sup> T cells in tumor and spleen, respectively, compared to the saline control. Furthermore, the same treatment also led to elevated levels of IFN- $\gamma$  and IL-2 in tumor and spleen (Figure 5B). A large number of IFN- $\gamma$ -secreting CD8<sup>+</sup> T cells, as well as higher levels of immunostimulatory cytokines related to Th1-type responses, were evidence of a shift of the tumor microenvironment from pro-oncogenic to antitumor.<sup>45</sup> Comparatively, injection with HCuSNPs-CpG alone induced less tumor IFN- $\gamma$ -secreting CD8<sup>+</sup> T cells and elevated lower IFN- $\gamma$  and IL-2 levels in tumor and spleen than did HCuSNPs-CpG plus laser treatment. Only a moderate increase of IFN- $\gamma$ -secreting CD8<sup>+</sup> T cells in tumor, but not in spleen, was observed in HCuSNPs-GpC plus laser group, suggesting photothermal therapy alone may only induce local antitumor effects.

Next, we examined whether HCuSNPs-CpG-mediated photothermal immunotherapy can exert systemic anti-tumor effects. First, we evaluated the *in vitro* tumor cell-lytic activities of splenocytes collected from the tumor-bearing mice following different treatments to test the effector function of cytotoxic T lymphocytes directly (Figure 6A). Among all treatment groups, HCuSNPs-CpG plus laser treatment induced the most pronounced cytotoxicity against EMT6 tumor cells at all three effector-to-target cell ratios. Significant cytotoxicity was also observed at effector-to-target cell ratios of 5:1 and 20:1 in HCuSNPs-CpG-treated group in comparison with that of free CpG-treated group. Photothermal therapy plus free CpG (HCuSNPs + laser + free CpG) treatment had similar effects on tumor cell-lytic activities as HCuSNPs-CpG treatment but was less effective than HCuSNPs-CpG plus laser treatment. Second, for evaluation of *in vivo* anti-tumor effects, we inoculated EMT6 tumors in the right flank (primary site) of mice and applied treatments at day 0 and day 6. The treated mice received another EMT6 tumor inoculation in the left flank (contralateral site) at day 6. Figure 6B demonstrates that intratumoral injection with free CpG did not exhibit significant antitumor activity at the primary sites, presumably because of its rapid clearance from the tumor. In contrast, groups treated with HCuSNPs-CpG alone or with HCuSNPs-GpC plus laser exhibited significant delays in tumor growth, indicating that either HCuSNPs-CpG-mediated immunotherapy alone or HCuSNPs-mediated photothermal therapy alone

can effectively relieve the primary tumor burden. A combined antitumor effect of photothermal therapy and immunotherapy was achieved by treating with HCuSNPs-CpG plus laser (Figure 6B). More importantly, this treatment significantly delayed growth of untreated tumors at distant contralateral sites. Notably, no distant tumors of the five tested mice in this treatment group grew until 10 days after inoculation (day 16). Neither photothermal therapy alone nor immunotherapy alone produced such an effect. Comparatively, photothermal therapy plus free CpG treatment did not show the combined antitumor effect at primary sites but at distant contralateral sites. This treatment significantly delayed distant tumor growth compared with saline, HCuSNPs-GpC plus laser (photothermal therapy alone), or free CpG treatments, while it did not show statistical difference in inhibition of distant tumors in comparison with HCuSNPs-CpG treatment ( $p = 0.083$ ). The inhibition of tumor growth at distant sites by photothermal therapy plus free CpG treatment was less effective than that treatment with HCuSNPs-CpG plus laser. Flow cytometric analysis confirmed that the number of IFN- $\gamma$ -secreting CD8<sup>+</sup> T cells in contralateral tumors in the group treated with HCuSNPs-CpG plus laser was 19-fold higher compared with saline-treated control (Figure S3). These results supported the notion that HCuSNPs-CpG-mediated photothermal immunotherapy can elicit systemic immunity not only against primary treated tumors but also against subsequent untreated tumors.

To determine whether the tumor-infiltrating T cells were specific for tumor-associated antigens, we used mice bearing EMT6 tumors transfected with ovalbumin (OVA, Figure S4). Notably, the CD8<sup>+</sup> T cells from the EMT6-OVA tumors treated with HCuSNPs-CpG plus laser were able to effectively produce IFN- $\gamma$  through *in vitro* induction by OVA (Figure S5), indicating this treatment can prime the cytotoxic T lymphocytes specific for antigens from the tumor cells. Comparatively, OVA induced fewer cytotoxic T lymphocytes from tumors treated with HCuSNPs-CpG but without laser. In the EMT6-OVA tumor model, we designed a "prime-boost" immunization strategy, in which the mice were primed with HCuSNPs-CpG, with or without laser, and boosted with OVA plus incomplete Freund's adjuvant (IFA). In comparison to conventional antigen immunization strategy, that is, priming with OVA plus complete Freund's adjuvant (CFA) and boosting with OVA plus IFA, prime immunization with HCuSNPs-CpG plus laser produced stronger anticancer effects against both primary and distant tumors (Figure 7). This result confirmed that treatment with HCuSNPs-CpG plus laser can induce high-level antigen-specific immune responses.

CpG immunotherapy has been studied as a strategy for tumor prevention and treatment.<sup>22–24</sup> Recent studies have characterized the immunotherapeutic significance of the combination of CpG immunotherapy and photodynamic therapy.<sup>46,47</sup> Photodynamic

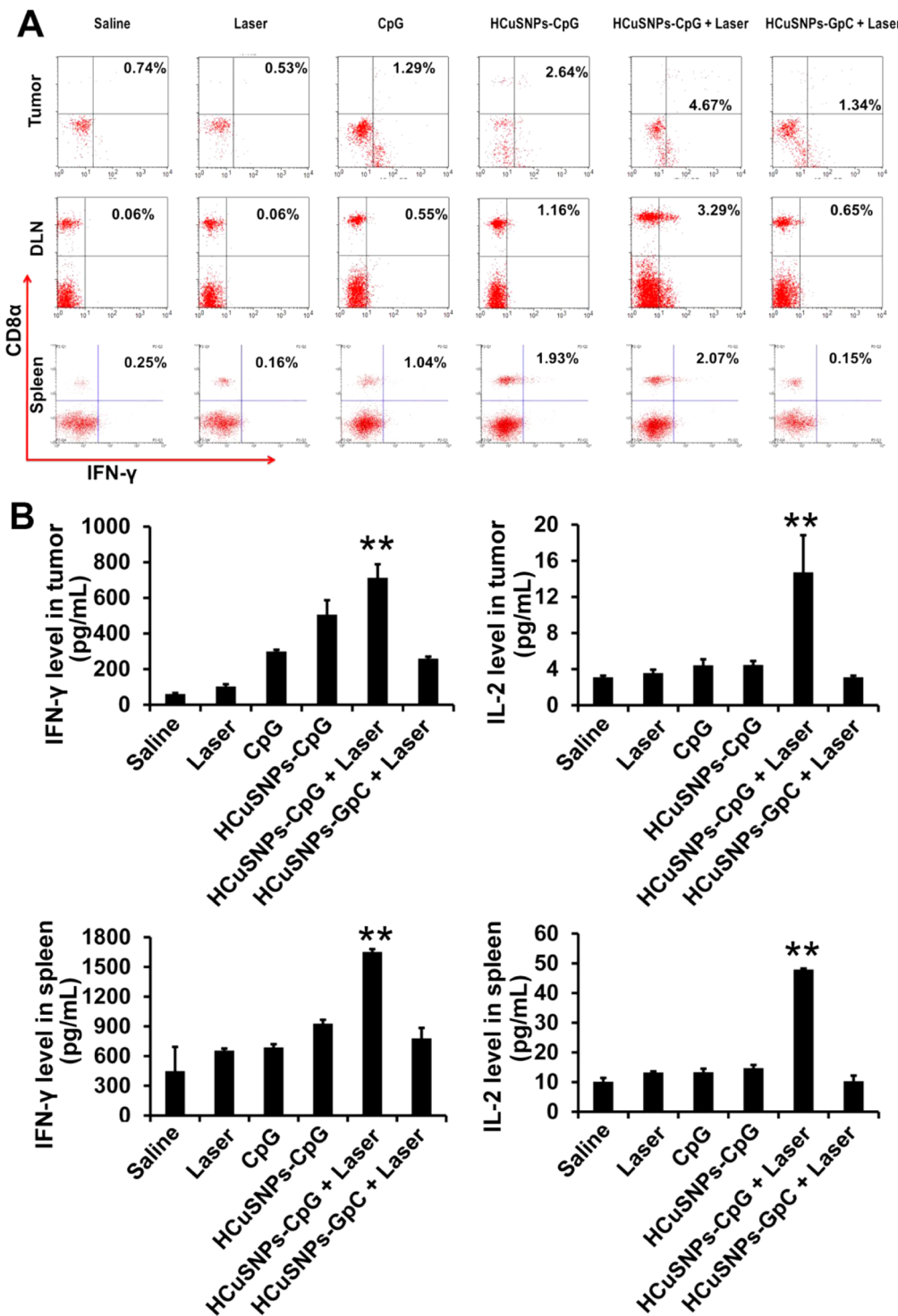


**Figure 5.** EMT6 tumor-bearing mice were given intratumoral injections of saline or different formulations containing  $100\text{ }\mu\text{g}$  of CpG or GpC (sham CpG control) with or without laser treatment ( $2.0\text{ W/cm}^2$ ,  $40\text{ s}$ ,  $900\text{ nm}$ ) at day 0 and day 6. (A) Flow cytometric analysis of intracellular IFN- $\gamma$  production by CD8 $^{+}$  T cells in tumor, tumor-draining lymph node or spleen at day 12 followed by CpG ( $20\text{ }\mu\text{g/mL}$ ) with or without mitomycin C-treated tumor cell stimulation *in vitro*. (B) ELISA analysis of IFN- $\gamma$  or IL-2 level in tumor or spleen following CpG ( $20\text{ }\mu\text{g/mL}$ ) stimulation *in vitro* at day 12. Significant difference (\*\* $p < 0.01$ ) between “HCuSNPs-CpG + Laser” group and other groups. Data shown are expressed as mean  $\pm$  SD ( $n = 3$ ). “HCuSNPs-GpC” represents HCuSNPs-chitosan-GpC conjugates.

therapy-induced cell lysates plus CpG oligodeoxy-nucleotides showed a significant suppression of tumor growth, both prophylactically and as therapy, compared to photodynamic therapy-induced cell lysates alone or free CpG alone.<sup>46</sup> The enhanced antitumor activity was

also observed when combining CpG immunotherapy with chemotherapy or radiotherapy.<sup>48–50</sup> Here, our results supported the hypothesis that the combined host antitumor immune responses are induced by photothermal immunotherapy in single settings, HCuSNPs-CpG,

through a near-infrared light-initiated transformation process. HCuSNPs-mediated photothermal therapy synergized with CpG-mediated immunotherapy, through which photothermal ablation destroyed primary (local) tumors and exposed tumor-associated antigens, and the photothermally triggered formation of chitosan-CpG nanocomplexes increased both innate and adaptive

immunity. The combination of photothermal therapy and immunotherapy displayed more effective systemic immunity against untreated tumors, compared to photothermal therapy or immunotherapy alone. It is noticeable that photothermal therapy-induced tumor cell death provided a source of tumor antigens released from the host's own tumor. As a result, each individually treated host produced an *in situ* autovaccine.<sup>17</sup> Current vaccine strategies (peptide or cDNA) have concentrated on a single and identified tumor-specific antigen.<sup>51</sup> Since tumor-specific antigens vary from tumor to tumor and from patient to patient, HCuSNPs-CpG-mediated photothermal immunotherapy, in lieu of current vaccine strategies, may have the potential to vaccinate patients against multiple tumor-specific antigens, tailored to an individual patient's tumor.

Our recently published data showed that systemically administrated pegylated HCuSNPs were eliminated through both hepatobiliary and renal excretion, resulting in approximate 90% of injected dose (% ID) of Cu cleared within 1 month postinjection.<sup>36</sup> Here, we tested the biodegradability of HCuSNPs-CpG through intratumoral injection, by examining Cu distribution in tumors and major organs. About 21% ID of Cu was cleared from tumors within 14 days after intratumoral injection with HCuSNPs-CpG (Figure 8A). In comparison, more than double amount of Cu (~47% ID) was eliminated from tumors following intratumoral injection with HCuSNPs-CpG plus laser treatment. This was possibly attributed to photothermally induced disintegration of the original ~85 nm HCuSNPs into ~10 nm small CuS nanoparticles, resulting in accelerated clearance from the tumor. There was no significant difference in Cu distribution in major organs of the intratumorally injected mice treated with or without laser. Liver retained the highest amount of Cu at 14 days following intratumoral injection in both treatment groups (Figure 8B). Quantitative analysis of Cu indicated that  $14.3 \pm 12.2\%$  ID of Cu appeared in feces

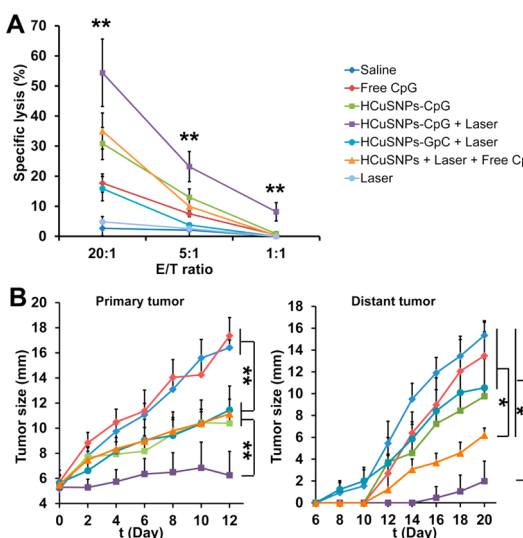


**Figure 6.** (A) EMT6 tumor-bearing mice were given intratumoral injection of saline or different formulations containing 100  $\mu$ g of CpG or GpC (sham CpG control) with or without laser treatment (2.0 W/cm<sup>2</sup>, 40 s, 900 nm) at day 0 and day 6. The splenocytes were collected at day 12 followed by mitomycin C-treated tumor cell and mIL-2 (5 U/mL) stimulation *in vitro*. Cytolytic activity of the splenocytes was determined by lactate dehydrogenase assay. "E/T ratio" represents effector/target cell ratio. Significant difference (\*\*p < 0.01) between "HCuSNPs-CpG + Laser" group and other treatment groups at E/T ratio of 1:1, 5:1, or 20:1. Data shown are expressed as mean  $\pm$  SD (n = 3). (B) Growth of the primary treated tumor and the distant (contralateral) untreated tumor over time. Data shown are expressed as mean  $\pm$  SD (n = 5). Significant difference between the compared groups (\*p < 0.05). "HCuSNPs-GpC" represents HCuSNPs-chitosan-GpC conjugates. "HCuSNPs + Laser + Free CpG" represents photothermal therapy plus free CpG treatment.

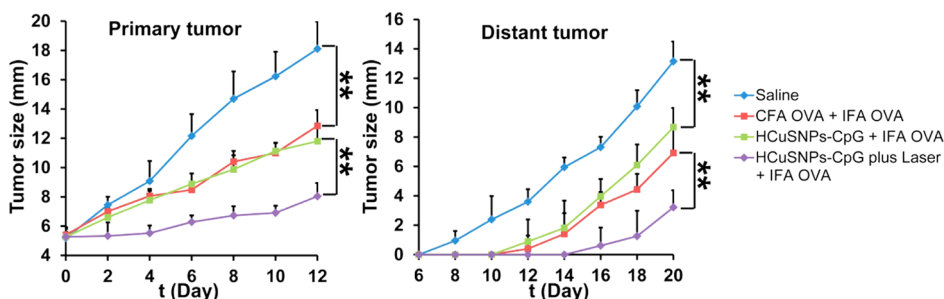


**Figure 7.** BALB/c mice bearing EMT6-OVA tumor in right flank were given the following treatment: group 1, intratumoral injection with saline at day 0 and day 6; group 2, intratumoral injection with OVA (50  $\mu$ g/mouse) with complete Freund's adjuvant (CFA) at day 0 and intratumoral injection with OVA (50  $\mu$ g/mouse) with incomplete Freund's adjuvant (IFA) at day 6; group 3, intratumoral injection with HCuSNPs-CpG (100  $\mu$ g/mouse) at day 0 and intratumoral injection with OVA (50  $\mu$ g/mouse) with IFA at day 6; group 4, intratumoral injection with HCuSNPs-CpG (100  $\mu$ g/mouse) plus laser (900 nm, 2.0 W/cm<sup>2</sup> for 40 s) at day 0 and intratumoral injection with OVA (50  $\mu$ g/mouse) with IFA at day 6. At day 6, the mice were subcutaneously inoculated with  $3 \times 10^5$  EMT6-OVA cells in left (contralateral) flank. Growth of primary treated tumor or contralateral untreated tumor over time is presented following the scheduled treatment with saline or different formulations. Data shown are expressed as mean  $\pm$  SD (n = 5). Significant difference between the compared groups (\*\*p < 0.01).

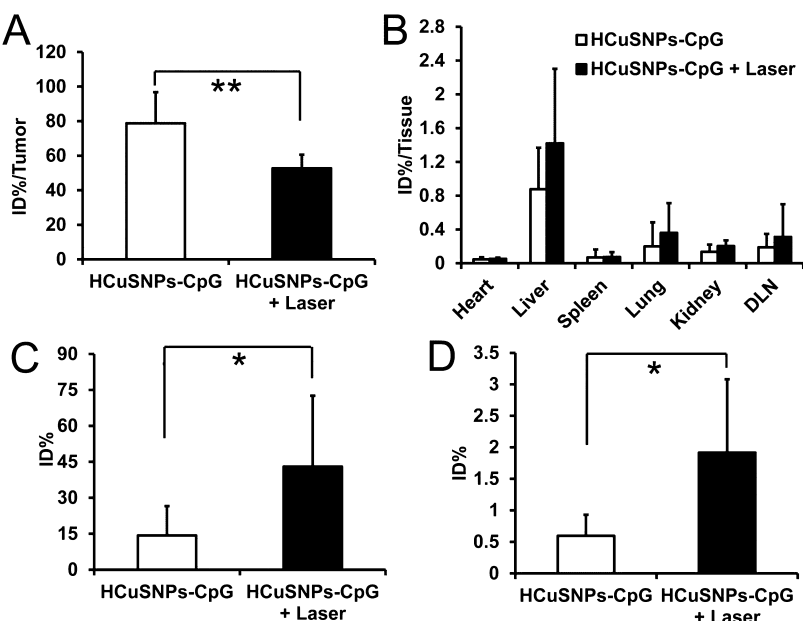


**Figure 8.** EMT6 tumor-bearing mice were given intratumoral injection of HCuSNPs-CpG containing 1 mg of Cu per mouse with or without laser treatment ( $2.0 \text{ W/cm}^2$ , 40 s, 900 nm) at day 0 and day 6. Biodistribution of Cu in tumors (A) and major organs (B) at day 14 following injection. “DLN” represents tumor-draining lymph node. Data are expressed as percentage of injected dose per tissue (% ID/tissue). Cumulative excreted Cu in feces (C) and urine (D) collected from day 0 to day 14. All data presented are the values subtracted from endogenous Cu content. Data are presented as mean  $\pm$  SD ( $n = 5$ ). Significant difference in groups between HCuSNPs-CpG and HCuSNPs-CpG plus laser (\* $p < 0.05$ ; \*\* $p < 0.01$ ).

within 14 days postinjection of HCuSNPs-CpG, while  $43.0 \pm 29.6\%$  ID of Cu was detected in feces from mice following HCuSNPs-CpG plus laser treatment (Figure 8C). Comparatively, only a small amount of Cu was cleared by kidney in both treatment groups (Figure 8D). Our results indicated that (1) intratumorally injected HCuSNPs-CpG can be cleared from the local injection site (tumor); (2) hepatobiliary excretion is the major clearance pathway of HCuSNPs-CpG from the body; (3) laser-triggered disintegration of HCuSNPs facilitates particle elimination.

## CONCLUSION

In this study, we described a near-infrared light-initiated transformative nano-CpG platform, HCuSNPs-CpG, for cancer photothermal immunotherapy in a

mouse model. Success of this technique relies on photothermally triggered disintegration of HCuSNPs, allowing the HCuSNPs-CpG conjugates to reassemble and transform into chitosan-CpG nanocomplexes. The chitosan-CpG nanocomplexes increase their tumor retention and promote CpG uptake by plasmacytoid dendritic cells. The HCuSNPs-CpG-mediated photothermal immunotherapy elicits more effective systemic immune responses than immunotherapy or photothermal therapy alone, resulting in combined anticancer effects against primary treated as well as distant untreated tumors. Strong anti-tumor effectiveness, combined with quick elimination, would seem to justify further development of this HCuSNPs conjugate-based photothermal immunotherapy.

## EXPERIMENTAL SECTION

**Materials.** The chemicals were purchased from Sigma-Aldrich Chemical, Inc. unless mentioned specifically. Female BALB/c mice (6–8 weeks old) were ordered from Jackson Laboratory, Inc. The mice were maintained in a pathogen-free environment, and all animal experiments were performed in compliance with the guidelines established by University of Rhode Island Institutional Animal Care and Use Committee (IACUC). EMT6 murine mammary carcinoma cell line was purchased from American Type Culture Collection (ATCC). EMT6 cells were cultured in Waymouth media supplemented with 10% heat-inactivated fetal bovine serum (FBS) and penicillin-streptomycin (Life Technologies). CpG oligodeoxynucleotide (ODN2216, 5'-ggGGGAGCATGCTGgggggc-3') was custom synthesized by Life Technologies, Inc. GpC oligodeoxynucleotide

(5'-ggGGGAGCATGCTGgggggc-3') was custom synthesized (Genscript) as sham CpG control.

**Preparation of HCuSNPs-CpG.** HCuSNPs were synthesized according to our previous report.<sup>36,52</sup> Thiolated chitosan was synthesized by modifying the previous method (see Supporting Information).<sup>53</sup> The thiolated chitosan (10 mg) was dissolved in 5 mL of distilled water to which 0.5 mL of HCuSNPs (2 mg of CuS) was added under constant stirring for 48 h. The HCuSNPs conjugated with thiolated chitosan (HCuSNPs-Chi) were centrifuged at 10 000 rpm for 8 min at room temperature and washed with distilled water. To formulate HCuSNPs-CpG, 0.1 mL of CpG aqueous solution (containing 10  $\mu\text{g}$  CpG) was added to 0.2 mL of the above HCuSNPs-Chi suspension (containing 200  $\mu\text{g}$  CuS) under stirring at room temperature.

**Laser Treatment of HCuSNPs-CpG *In Vitro*.** HCuSNPs-CpG aqueous suspension (90  $\mu\text{L}$  containing 0.9  $\mu\text{g}$  of CpG) was irradiated with

a pulsed near-infrared laser centered at 900 nm ( $2.0 \text{ W/cm}^2$ ) for different times. The 900 nm near-infrared laser was generated from a master oscillator power amplifier (MOPA)  $\text{Ti}^{3+}$ :sapphire tunable laser (LT-2211A, LOTIS TII) pumped by a pulsed Q-switched Nd:YAG laser system (LS-2137/2, LOTIS TII). After laser treatment, the suspension was centrifuged at 3000 rpm for 5 min, which allowed complete precipitation of the CuS nanoparticles. Both pellet and supernatant were collected separately for agarose gel electrophoresis: 0.8% agarose; 1 × TAE; loading buffer (30% glycerol, 0.025% xylene cyanol, 0.025% bromophenol blue). The gel was run at 75 V for 30 min and then stained with 1:10000 dilution of SYBR Green II (Life Technologies) for 20 min. Washed with water, the gel was scanned under Typhoon FLA9000 scanner (GE Healthcare).

**HCuSNPs-CpG Distribution.** For *in vivo* tracking the distribution of CpG, CpG modified with a primary amine group at the 5' terminal through the C<sub>6</sub> linker (5'-NH<sub>2</sub>-C<sub>6</sub>-CpG-3') was custom synthesized (Genscript). The amine-modified CpG (100  $\mu\text{g}$ ) was added to 100  $\mu\text{g}$  of IRDye680RD NHS ester (LiCor) in PBS (pH 7.4) for overnight reaction. The product was passed through a PD-10 column (Sigma) to separate the unreacted dye. The purified CpG-IRDye680 (fCpG) conjugate was lyophilized and stored at -20 °C until use. The CpG-IRDye680-loaded HCuSNPs (HCuSNPs-fCpG) were prepared with the same method as used for HCuSNPs-CpG.

BALB/c mice were subcutaneously (sc) inoculated with 1 × 10<sup>6</sup> EMT6 cells in the right flank. When the tumor size reached 8–10 mm, the tumor-bearing mice were divided into three groups ( $n = 3$ ). Mice in group 1 were intratumorally injected with 50  $\mu\text{L}$  of free fCpG (10  $\mu\text{g}$  fCpG/mouse). Mice in groups 2 and 3 were intratumorally injected with 50  $\mu\text{L}$  of HCuSNPs-fCpG (10  $\mu\text{g}$  fCpG/mouse). At 30 min after injection, tumors of mice in group 3 received near-infrared laser irradiation (900 nm, 2.0  $\text{W/cm}^2$ , 40 s). All the mice were imaged by live small animal optical imaging system (IVIS Lumina XR, Caliper) at 1, 4, or 24 h following injection. Twenty-four hours after injection, the mice were euthanized. The tumor and the draining lymph nodes were harvested for imaging.

Following imaging, the tumor tissues were embedded in Tissue-Tek O.C.T compound (Sakura Finetek) for cryosectioning (8  $\mu\text{m}$  thickness). The immunohistochemistry was performed by staining with rat anti-mouse plasmacytoid dendritic cell monoclonal antibody (clone 120G8.04, Imgenex, 1:50) followed by Alexa Flour 488-conjugated goat anti-rat IgG (Life Technologies, 1:750). The cell nuclei were counterstained with 4',6-diamidino-2-phenylindole (DAPI, Sigma).

**Tumor Treatment.** BALB/c mice bearing the EMT6 tumor were used to investigate the efficacy of antitumor immunity. The mice were sc inoculated with 1 × 10<sup>6</sup> EMT6 cells in the right flank at day -4. The tumor size reached 4–6 mm at day 0. The mice were then divided into 6 groups and received the following treatment at day 0: intratumoral injection of saline; laser alone; intratumoral injection of free CpG (100  $\mu\text{g}$ ) alone; intratumoral injection of HCuSNPs-CpG (100  $\mu\text{g}$  of CpG) alone; intratumoral injection of HCuSNPs-CpG (100  $\mu\text{g}$  of CpG) plus laser; intratumoral injection of HCuSNPs-GpC (sham CpG control, 100  $\mu\text{g}$  of GpC) plus laser; intratumoral injection of HCuSNPs plus laser followed by intratumoral injection of free CpG (100  $\mu\text{g}$ ) 3 h after the laser treatment (photothermal therapy plus free CpG). For laser treatment groups, the mice received near-infrared laser irradiation (900 nm, 2.0  $\text{W/cm}^2$ , 40 s) at 30 min after injection. A boost treatment with same dose was given to each group at day 6. Also at day 6, the mice were sc injected with 3 × 10<sup>5</sup> EMT6 cells in the left flank. Tumor size was assessed by measuring the length and width and calculated with the standard formula: tumor size = (length + width)/2.

**Immunohistochemistry.** For staining the activated NK cells, tumors were collected at day 8 for cryosectioning. The sections were stained with FITC-conjugated anti-mouse CD69 (1:50, eBioscience) and APC-conjugated anti-mouse CD49b (1:50, eBioscience) followed by DAPI counterstaining.

**Cytokine Assay.** Spleen and tumor tissues were collected at day 12. Single cell suspension was prepared as described above. The cells were then incubated with CpG (20  $\mu\text{g/mL}$ ) in 6-well plates. The supernatant was collected after 8 h incubation. The IFN- $\gamma$  and IL-2 concentrations were tested with ELISA (eBioscience) according to the manufacturer's protocol.

**Cytotoxicity Assay of Cytotoxic T Lymphocytes.** A lactate dehydrogenase (LDH) assay was used to evaluate the cytotoxicity of cytotoxic T lymphocytes according to the previous method.<sup>54</sup> The splenocytes collected at day 12 from tumor-bearing mice were stimulated with mitomycin C-treated tumor cells and mouse IL-2 for 72 h at 37 °C under 5% CO<sub>2</sub>. After stimulation, viable splenocytes were counted and used as effector cells for the measurement of specific cytolytic activity. The EMT6 cells, as target cells, were distributed into triplicate wells of a 96-well plate (2 × 10<sup>4</sup> cells/well) in 100  $\mu\text{L}$  of complete RPMI-1640 medium supplemented with 2% FBS. The stimulated lymphocytes were diluted in the same medium and added to target cells in triplicate with (effector-to-target) E/T cell ratios of 20:1, 5:1, and 1:1 in a total volume of 200  $\mu\text{L}$ . Wells added with only target cells served as spontaneous release. Target cells were treated with lysis buffer to calculate maximal release of LDH. The cell mixtures were incubated for 6 h at 37 °C under 5% CO<sub>2</sub>. After incubation, the supernatant was collected and assayed for LDH according to the manufacturer's instructions (Sigma).

**Tumor Growth Delay Study.** BALB/c mice bearing EMT6 tumors in the right flank, with tumor sizes of 4–6 mm ( $n = 5$ , defined as day 0), were used for evaluation of the antitumor efficacy with the following treatments at day 0: intratumoral injection of saline; intratumoral injection of free CpG (100  $\mu\text{g}$ ) alone; intratumoral injection of HCuSNPs-CpG (100  $\mu\text{g}$  of CpG) alone; intratumoral injection of HCuSNPs-CpG (100  $\mu\text{g}$  of CpG) plus laser; intratumoral injection of HCuSNPs-GpC (sham CpG control, 100  $\mu\text{g}$  of GpC) plus laser; intratumoral injection of HCuSNPs plus laser followed by intratumoral injection of free CpG (100  $\mu\text{g}$ ) 3 h after the laser treatment (photothermal therapy plus free CpG). For laser treatment groups, the mice received near-infrared laser irradiation (900 nm, 2.0  $\text{W/cm}^2$ , 40 s) at 30 min after injection. A boost treatment with same dose was given to each group at day 6. Also at day 6, the mice were sc injected with 3 × 10<sup>5</sup> EMT6 cells in the left flank. Tumor size was assessed by measuring the length and width and calculated with the standard formula: tumor size = (length + width)/2.

EMT6-OVA tumor-bearing mice were used to assess antigen-specific antitumor efficacies of different treatments. Briefly, 1 × 10<sup>6</sup> EMT6-OVA cells were sc inoculated in the right flank of the mice. When tumor size reached 4–6 mm, defined as day 0, the mice were divided into 4 groups ( $n = 5$ ) and received the following treatments: group 1, intratumoral injection with saline at day 0 and day 6; group 2, intratumoral injection with OVA (50  $\mu\text{g}/\text{mouse}$ ) in complete Freund's adjuvant (CFA) at day 0 and intratumoral injection with OVA (50  $\mu\text{g}/\text{mouse}$ ) in incomplete Freund's adjuvant (IFA) at day 6;<sup>55</sup> group 3, intratumoral injection with HCuSNPs-CpG (100  $\mu\text{g}/\text{mouse}$ ) at day 0 and intratumoral injection with OVA (50  $\mu\text{g}/\text{mouse}$ ) in IFA at day 6; group 4, intratumoral injection with HCuSNPs-CpG (100  $\mu\text{g}/\text{mouse}$ ) plus laser (900 nm, 2.0  $\text{W/cm}^2$  for 40 s) at day 0 and intratumoral injection with OVA (50  $\mu\text{g}/\text{mouse}$ ) in IFA at day 6. At day 6, 3 × 10<sup>5</sup> EMT6-OVA cells were inoculated in the left flank of the immunized mice. The tumor size was measured as described above.

**Biodistribution and Elimination of Cu.** BALB/c mice bearing EMT6 tumors in the right flank, with tumor sizes of 4–6 mm at day 0, were divided into three groups ( $n = 5$ ). Mice in groups 1 and 2 were intratumorally injected with HCuSNPs-CpG (1 mg of Cu per mouse). Mice in group 1 were treated with laser (900 nm, 2.0  $\text{W/cm}^2$ , 40 s) at 30 min after injection and at day 6. Mice in group 3 without injection were used as control for endogenous Cu. All mice were transferred to mouse metabolic cages (Tecniplast) for urine and feces collection up to 14 days.

At day 14, all mice were euthanized. The heart, liver, spleen, lung, kidney, tumor, and tumor-draining lymph nodes were collected. Tissue, urine, and feces samples were digested for the inductively coupled plasma mass spectrometer (ICP-MS) (model: X7, Thermo Electron Corporation) quantitative analysis of Cu according to our previously reported procedure.<sup>36</sup> Data of both HCuSNPs-CpG treatment groups were calculated by subtracting endogenous Cu content from the measured Cu values.

**Statistical Analysis.** The statistical difference of the results among multiple treatment groups was evaluated by one-way analysis of variance (ANOVA) followed by LSD *post hoc* multiple comparison tests. Differences in values of Cu biodistribution between two treatment groups were assessed using an unpaired Student's *t* test; *p* < 0.05 was considered significant.

**Conflict of Interest:** The authors declare no competing financial interest.

**Acknowledgment.** The authors thank R. Rodgers for editing the manuscript, R. Kingsley for assisting in transmission electron microscopy studies, A. Ahmed and A. Kim for assisting in ICP-MS analysis, and A. Slitt for offering us to use metabolic caging system. This work was supported in part by grants from the National Institutes of Health (P20GM103430, R01EB018748, P20GM104937 and R15AT007705), and by The Program for Professor of Special Appointment (Eastern Scholar) at Shanghai Institutions of Higher Learning (No.2012-05). Flow cytometric analysis was supported in part by the National Science Foundation EPSCoR Cooperative Agreement #EPS-1004057.

**Supporting Information Available:** Flow cytometric analysis of CD69<sup>+</sup> cells in lymphocyte population in tumor; flow cytometric analysis of plasmacytoid dendritic cells in tumor or draining lymph nodes; flow cytometric analysis of intracellular IFN- $\gamma$  production by CD8<sup>+</sup> T cells in the contralateral tumor; Western blot analysis of OVA expression in EMT6-OVA cells; flow cytometric analysis of intracellular IFN- $\gamma$  production by CD8<sup>+</sup> T cells in tumor following OVA stimulation. This material is available free of charge via the Internet at <http://pubs.acs.org>.

## REFERENCES AND NOTES

- Paiva, M. B.; Blackwell, K. E.; Saxton, R. E.; Bublik, M.; Liu, C. D.; Paiva Paolini, A. A.; Calcaterra, T. C.; Castro, D. J. Nd: YAG Laser Therapy for Palliation of Recurrent Squamous Cell Carcinomas in the Oral Cavity. *Lasers Surg. Med.* **2002**, *31*, 64–69.
- Paiva, M. B.; Blackwell, K. E.; Saxton, R. E.; Calcaterra, T. C.; Ward, P. H.; Soudant, J.; Castro, D. J. Palliative Laser Therapy for Recurrent Head and Neck Cancer: A Phase II Clinical Study. *Laryngoscope* **1998**, *108*, 1277–1283.
- Hirsch, L. R.; Stafford, R. J.; Bankson, J. A.; Sershen, S. R.; Rivera, B.; Price, R. E.; Hazle, J. D.; Halas, N. J.; West, J. L. Nanoshell-Mediated Near-Infrared Thermal Therapy of Tumors under Magnetic Resonance Guidance. *Proc. Natl. Acad. Sci. U.S.A.* **2003**, *100*, 13549–13554.
- Dickerson, E. B.; Dreaden, E. C.; Huang, X.; El-Sayed, I. H.; Chu, H.; Pushpanketh, S.; McDonald, J. F.; El-Sayed, M. A. Gold Nanorod Assisted Near-Infrared Plasmonic Photothermal Therapy (PPTT) of Squamous Cell Carcinoma in Mice. *Cancer Lett.* **2008**, *269*, 57–66.
- Chen, J.; Glauz, C.; Laforest, R.; Zhang, Q.; Yang, M.; Gidding, M.; Welch, M. J.; Xia, Y. Gold Nanocages as Photothermal Transducers for Cancer Treatment. *Small* **2010**, *6*, 811–817.
- Skrabalak, S. E.; Chen, J.; Au, L.; Lu, X.; Li, X.; Xia, Y. Gold Nanocages for Biomedical Applications. *Adv. Mater.* **2007**, *19*, 3177–3184.
- Lu, W.; Xiong, C.; Zhang, G.; Huang, Q.; Zhang, R.; Zhang, J. Z.; Li, C. Targeted Photothermal Ablation of Murine Melanomas with Melanocyte-Stimulating Hormone Analog-Conjugated Hollow Gold Nanospheres. *Clin. Cancer Res.* **2009**, *15*, 876–886.
- Kam, N. W.; O'Connell, M.; Wisdom, J. A.; Dai, H. Carbon Nanotubes as Multifunctional Biological Transporters and Near-Infrared Agents for Selective Cancer Cell Destruction. *Proc. Natl. Acad. Sci. U.S.A.* **2005**, *102*, 11600–11605.
- Li, Y.; Lu, W.; Huang, Q.; Huang, M.; Li, C.; Chen, W. Copper Sulfide Nanoparticles for Photothermal Ablation of Tumor Cells. *Nanomedicine* **2010**, *5*, 1161–1171.
- Song, S.; Xiong, C.; Zhou, M.; Lu, W.; Huang, Q.; Ku, G.; Zhao, J.; Flores, L. G., Jr.; Ni, Y.; Li, C. Small-Animal PET of Tumor Damage Induced by Photothermal Ablation with <sup>64</sup>Cu-Bis-Dota-Hypericin. *J. Nucl. Med.* **2011**, *52*, 792–799.
- Tian, Q.; Jiang, F.; Zou, R.; Liu, Q.; Chen, Z.; Zhu, M.; Yang, S.; Wang, J.; Hu, J. Hydrophilic Cu<sub>9</sub>S<sub>5</sub> Nanocrystals: A Photothermal Agent with a 25.7% Heat Conversion Efficiency for Photothermal Ablation of Cancer Cells *In Vivo*. *ACS Nano* **2011**, *5*, 9761–9771.
- Tian, Q.; Tang, M.; Sun, Y.; Zou, R.; Chen, Z.; Zhu, M.; Yang, S.; Wang, J.; Wang, J.; Hu, J. Hydrophilic Flower-like CuS Superstructures as an Efficient 980 nm Laser-Driven Photothermal Agent for Ablation of Cancer Cells. *Adv. Mater.* **2011**, *23*, 3542–3547.
- Zhou, M.; Zhang, R.; Huang, M.; Lu, W.; Song, S.; Melancon, M. P.; Tian, M.; Liang, D.; Li, C. A Chelator-Free Multifunctional [<sup>64</sup>Cu]CuS Nanoparticle Platform for Simultaneous Micro-PET/CT Imaging and Photothermal Ablation Therapy. *J. Am. Chem. Soc.* **2010**, *132*, 15351–15358.
- Pilot Study of Aurolase(Tm) Therapy in Refractory and/or Recurrent Tumors of the Head and Neck; <http://clinicaltrials.gov/show/NCT00848042>.
- Efficacy Study of Aurolase Therapy in Subjects with Primary and/or Metastatic Lung Tumors; <http://clinicaltrials.gov/show/NCT01679470>.
- Chen, W. R.; Singhal, A. K.; Liu, H.; Nordquist, R. E. Antitumor Immunity Induced by Laser Immunotherapy and Its Adoptive Transfer. *Cancer Res.* **2001**, *61*, 459–461.
- Naylor, M. F.; Chen, W. R.; Teague, T. K.; Perry, L. A.; Nordquist, R. E. *In Situ* Photoimmunotherapy: A Tumour-Directed Treatment for Melanoma. *Br. J. Dermatol.* **2006**, *155*, 1287–1292.
- Hodge, J. W.; Guha, C.; Neefjes, J.; Gulley, J. L. Synergizing Radiation Therapy and Immunotherapy for Curing Incurable Cancers. Opportunities and Challenges. *Oncology* **2008**, *22*, 1064–1070.
- Krieg, A. M. Therapeutic Potential of Toll-like Receptor 9 Activation. *Nat. Rev. Drug Discovery* **2006**, *5*, 471–484.
- Iwasaki, A.; Medzhitov, R. Toll-like Receptor Control of the Adaptive Immune Responses. *Nat. Immunol.* **2004**, *5*, 987–995.
- Vollmer, J.; Krieg, A. M. Immunotherapeutic Applications of CpG Oligodeoxynucleotide TLR9 Agonists. *Adv. Drug Delivery Rev.* **2009**, *61*, 195–204.
- Bode, C.; Zhao, G.; Steinhagen, F.; Kinjo, T.; Klinman, D. M. CpG DNA as a Vaccine Adjuvant. *Expert Rev. Vaccines* **2011**, *10*, 499–511.
- Krieg, A. M. Toll-like Receptor 9 (TLR9) Agonists in the Treatment of Cancer. *Oncogene* **2008**, *27*, 161–167.
- Murad, Y. M.; Clay, T. M. CpG Oligodeoxynucleotides as TLR9 Agonists: Therapeutic Applications in Cancer. *BioDrugs* **2009**, *23*, 361–375.
- Wilson, K. D.; de Jong, S. D.; Tam, Y. K. Lipid-Based Delivery of CpG Oligonucleotides Enhances Immunotherapeutic Efficacy. *Adv. Drug Delivery Rev.* **2009**, *61*, 233–242.
- Bourquin, C.; Anz, D.; Zwiorek, K.; Lanz, A. L.; Fuchs, S.; Weigel, S.; Wurzenberger, C.; von der Borch, P.; Golic, M.; Moder, S.; et al. Targeting CpG Oligonucleotides to the Lymph Node by Nanoparticles Elicits Efficient Antitumoral Immunity. *J. Immunol.* **2008**, *181*, 2990–2998.
- Chikh, G.; de Jong, S. D.; Sekirov, L.; Raney, S. G.; Kazem, M.; Wilson, K. D.; Cullis, P. R.; Dutz, J. P.; Tam, Y. K. Synthetic Methylated CpG ODNs Are Potent *In Vivo* Adjuvants When Delivered in Liposomal Nanoparticles. *Int. Immunopharmacol.* **2009**, *21*, 757–767.
- de Jong, S. D.; Basha, G.; Wilson, K. D.; Kazem, M.; Cullis, P.; Jefferies, W.; Tam, Y. The Immunostimulatory Activity of Unmethylated and Methylated CpG Oligodeoxynucleotide Is Dependent on Their Ability to Colocalize with TLR9 in Late Endosomes. *J. Immunol.* **2010**, *184*, 6092–6102.
- Malyala, P.; O'Hagan, D. T.; Singh, M. Enhancing the Therapeutic Efficacy of CpG Oligonucleotides Using

- Biodegradable Microparticles. *Adv. Drug Delivery Rev.* **2009**, *61*, 218–225.
30. Schreiber, H. A.; Prechl, J.; Jiang, H.; Zozulya, A.; Fabry, Z.; Denes, F.; Sandor, M. Using Carbon Magnetic Nanoparticles To Target, Track, and Manipulate Dendritic Cells. *J. Immunol. Methods* **2010**, *356*, 47–59.
  31. Zhao, D.; Alizadeh, D.; Zhang, L.; Liu, W.; Farrukh, O.; Manuel, E.; Diamond, D. J.; Badie, B. Carbon Nanotubes Enhance CpG Uptake and Potentiate Antiglioma Immunity. *Clin. Cancer Res.* **2010**, *17*, 771–782.
  32. Fan, H.; Zhang, I.; Chen, X.; Zhang, L.; Wang, H.; Da Fonseca, A.; Manuel, E. R.; Diamond, D. J.; Raubitschek, A.; Badie, B. Intracerebral CpG Immunotherapy with Carbon Nanotubes Abrogates Growth of Subcutaneous Melanomas in Mice. *Clin. Cancer Res.* **2012**, *18*, 5628–5638.
  33. Kim, J. H.; Noh, Y. W.; Heo, M. B.; Cho, M. Y.; Lim, Y. T. Multifunctional Hybrid Nanoconjugates for Efficient *In Vivo* Delivery of Immunomodulating Oligonucleotides and Enhanced Antitumor Immunity. *Angew. Chem., Int. Ed.* **2012**, *51*, 9670–9673.
  34. Lin, A. Y.; Almeida, J. P.; Bear, A.; Liu, N.; Luo, L.; Foster, A. E.; Drezek, R. A. Gold Nanoparticle Delivery of Modified CpG Stimulates Macrophages and Inhibits Tumor Growth for Enhanced Immunotherapy. *PLoS One* **2013**, *8*, e63550.
  35. Wei, M.; Chen, N.; Li, J.; Yin, M.; Liang, L.; He, Y.; Song, H.; Fan, C.; Huang, Q. Polyvalent Immunostimulatory Nanoagents with Self-Assembled CpG Oligonucleotide-Conjugated Gold Nanoparticles. *Angew. Chem., Int. Ed.* **2012**, *51*, 1202–1206.
  36. Guo, L.; Pandari, I.; Yan, D. D.; Szulak, K.; Li, Y.; Chen, Y. T.; Ma, H.; Niesen, D. B.; Seeram, N.; Ahmed, A.; et al. A Comparative Study of Hollow Copper Sulfide Nanoparticles and Hollow Gold Nanospheres on Degradability and Toxicity. *ACS Nano* **2013**, *7*, 8780–8793.
  37. Takahashi, H.; Niidome, Y.; Yamada, S. Controlled Release of Plasmid DNA from Gold Nanorods Induced by Pulsed Near-Infrared Light. *Chem. Commun.* **2005**, 2247–2249.
  38. Chen, C. C.; Lin, Y. P.; Wang, C. W.; Tzeng, H. C.; Wu, C. H.; Chen, Y. C.; Chen, C. P.; Chen, L. C.; Wu, Y. C. DNA-Gold Nanorod Conjugates for Remote Control of Localized Gene Expression by Near Infrared Irradiation. *J. Am. Chem. Soc.* **2006**, *128*, 3709–3715.
  39. Lu, W.; Zhang, G.; Zhang, R.; Flores, L. G., II; Huang, Q.; Gelovani, J. G.; Li, C. Tumor Site-Specific Silencing of Nf- $\kappa$ b P65 by Targeted Hollow Gold Nanosphere-Mediated Photothermal Transfection. *Cancer Res.* **2010**, *70*, 3177–3188.
  40. Wheeler, D. A.; Newhouse, R. J.; Wang, H. N.; Zou, S. L.; Zhang, J. Z. Optical Properties and Persistent Spectral Hole Burning of Near Infrared-Absorbing Hollow Gold Nanospheres. *J. Phys. Chem. C* **2010**, *114*, 18126–18133.
  41. Zhu, H.; Wang, J.; Wu, D. Fast Synthesis, Formation Mechanism, and Control of Shell Thickness of CuS Hollow Spheres. *Inorg. Chem.* **2009**, *48*, 7099–7104.
  42. Kim, J. S.; Kim, H. J. Matrix-Assisted Laser Desorption/Ionization Time-of-Flight Mass Spectrometric Observation of a Peptide Triplet Induced by Thermal Cleavage of Cystine. *Rapid Commun. Mass Spectrom.* **2001**, *15*, 2296–2300.
  43. Liu, C.; Lou, Y.; Lizée, G.; Qin, H.; Liu, S.; Rabinovich, B.; Kim, G. J.; Wang, Y. H.; Ye, Y.; Sikora, A. G.; et al. Plasmacytoid Dendritic Cells Induce NK Cell-Dependent, Tumor Antigen-Specific T Cell Cross-Priming and Tumor Regression in Mice. *J. Clin. Invest.* **2008**, *118*, 1165–1175.
  44. Sasai, M.; Linehan, M. M.; Iwasaki, A. Bifurcation of Toll-like Receptor 9 Signaling by Adaptor Protein 3. *Science* **2010**, *329*, 1530–1534.
  45. Kortylewski, M.; Swiderski, P.; Herrmann, A.; Wang, L.; Kowollik, C.; Kujawski, M.; Lee, H.; Scuto, A.; Liu, Y.; Yang, C.; et al. *In Vivo* Delivery of SiRNA to Immune Cells by Conjugation to a TLR9 Agonist Enhances Antitumor Immune Responses. *Nat. Biotechnol.* **2009**, *27*, 925–932.
  46. Bae, S. M.; Kim, Y. W.; Kwak, S. Y.; Ro, D. Y.; Shin, J. C.; Park, C. H.; Han, S. J.; Oh, C. H.; Kim, C. K.; Ahn, W. S. Photodynamic Therapy-Generated Tumor Cell Lysates with CpG-Oligodeoxynucleotide Enhance Immunotherapy Efficacy in Human Papillomavirus 16 (E6/E7) Immortalized Tumor Cells. *Cancer Sci.* **2007**, *98*, 747–752.
  47. Xia, Y.; Gupta, G. K.; Castano, A. P.; Mroz, P.; Avci, P.; Hamblin, M. R. CpG Oligodeoxynucleotide as Immune Adjuvant Enhances Photodynamic Therapy Response in Murine Metastatic Breast Cancer. *J. Biophotonics* **2013**, 10.1002/jbio.201300072.
  48. Milas, L.; Mason, K. A.; Ariga, H.; Hunter, N.; Neal, R.; Valdecana, D.; Krieg, A. M.; Whisnant, J. K. CpG Oligodeoxynucleotide Enhances Tumor Response to Radiation. *Cancer Res.* **2004**, *64*, 5074–5077.
  49. Mason, K. A.; Neal, R.; Hunter, N.; Ariga, H.; Ang, K.; Milas, L. CpG Oligodeoxynucleotides Are Potent Enhancers of Radio- and Chemoresponses of Murine Tumors. *Radiother. Oncol.* **2006**, *80*, 192–198.
  50. Mason, K. A.; Hunter, N. R. CpG Plus Radiotherapy: A Review of Preclinical Works Leading to Clinical Trial. *Front. Oncol.* **2012**, *2*, 101.
  51. Copier, J.; Dalgleish, A. Overview of Tumor Cell-Based Vaccines. *Int. Rev. Immunol.* **2006**, *25*, 297–319.
  52. Ramadan, S.; Guo, L.; Li, Y.; Yan, B.; Lu, W. Hollow Copper Sulfide Nanoparticle-Mediated Transdermal Drug Delivery. *Small* **2012**, *8*, 3143–3150.
  53. Lee, D.; Zhang, W.; Shirley, S. A.; Kong, X.; Hellermann, G. R.; Lockey, R. F.; Mohapatra, S. S. Thiolated Chitosan/DNA Nanocomplexes Exhibit Enhanced and Sustained Gene Delivery. *Pharm. Res.* **2007**, *24*, 157–167.
  54. Pouyanfar, S.; Bamdad, T.; Hashemi, H.; Bandehpour, M.; Kazemi, B. Induction of Protective Anti-Ctl Epitope Responses against Her-2-Positive Breast Cancer Based on Multivalent T7 Phage Nanoparticles. *PLoS One* **2012**, *7*, e49539.
  55. Ejrnaes, M.; Videbaek, N.; Christen, U.; Cooke, A.; Michelsen, B. K.; von Herrath, M. Different Diabetogenic Potential of Autoaggressive CD8<sup>+</sup> Clones Associated with IFN-gamma-Inducible Protein 10 (CXC Chemokine Ligand 10) Production but Not Cytokine Expression, Cytolytic Activity, or Homing Characteristics. *J. Immunol.* **2005**, *174*, 2746–2755.